

Table S1:  $\delta^{15}\text{N}$  values and elemental composition of *Tillandsia landbeckii* plant material analysed in this study.

No	Sample locality <sup>a</sup>	Elevation (m a.s.l.)	$\delta^{15}\text{N}$ (‰)	N (%)	OC (%)	S (%)	active/dead
1	PCRUC-1	1000	-16.92	1.7	44.8	0.1	A
2	PCRUC-2	1000	-17.62	1.4	45.5	0.1	A
3	PCRUC-3	1000	-15.44	1.4	45.1	0.2	A
4	PCRUC-4	1000	-14.31	1.3	44.4	0.1	A
5	QVIT-1	1027	-8.60	0.3	33.7	0.7	A
6	QVIT-2	1027	-9.75	0.5	40.4	0.4	A
7	QVIT-3	1058	-9.61	0.6	37.6	0.6	A
8	QVIT-4	1058	-8.57	0.5	38.3	0.6	A
9	QCAM-1	1070	-10.22	0.3	37.2	0.5	A
10	QCAM-2	1080	-7.09	0.3	29.5	0.8	A
11	QCAM-3	1090	-7.03	0.4	27.2	0.8	A
12	QCAM-4	1100	-8.75	0.3	28.0	0.6	A
13	QCAM-5	1110	-6.87	0.4	26.4	1.0	A
14	QCAM-6	1120	-5.67	0.2	25.7	1.5	A
15	QCAM-7	1130	-8.38	0.3	28.0	1.0	A
16	CGUA-1	1040	-4.65	0.6	35.5	0.6	A
17	CGUA-2	1085	-3.22	0.3	35.8	0.5	A
18	CGUA-3	1085	-6.65	0.3	34.9	0.5	A
19	CGUA-4	1072	-5.83	0.3	39.1	0.6	A
20	CGUA-6	1055	-4.51	0.4	40.0	0.4	A
21	CGUA-8	1059	-5.57	0.3	40.1	0.6	A
22	CGUA-9	1062	-5.72	0.4	40.4	0.4	A
23	CGUA-10	1077	-4.13	0.2	35.4	0.8	A
24	COYA-1	1215	-2.90	0.5	43.3	0.3	A
25	COYA-3	1185	-2.64	0.6	35.8	0.7	A
26	COYA-4	1170	-1.85	0.5	40.1	0.2	A
27	COYA-5	1155	-2.73	0.5	42.1	0.3	A
28	COYA-7	1125	-1.49	0.3	39.1	0.2	A
29	COYA-8	1110	-0.76	0.4	44.3	0.3	A
30	COYA-10	1088	1.01	0.3	39.2	0.7	A
31	CPAJ-1	971	0.47	0.5	40.3	0.4	A
32	CPAJ-2	974	0.40	0.5	39.0	0.4	A
33	CPAJ-3	976	1.57	0.4	26.7	1.3	A
34	CPAJ-4	966	-1.00	0.5	43.1	0.2	A
35	CPAJ-6	1060	0.20	0.5	40.3	0.2	A
36	CPAJ-8	1040	1.29	0.7	31.2	1.0	A
37	CPAJ-9	1030	0.30	0.4	39.0	0.4	A
38	CPAJ-11	1010	1.26	0.4	42.8	0.3	A
39	CPAJ-12	1000	1.07	0.4	41.5	0.4	A
40	CPAJ-13A	1041	1.29	0.4	39.1	0.4	A
41	CPAJ-13B	1041	4.57	0.5	39.2	0.3	D
42	CPAJ-16	1010	2.01	0.3	41.1	0.3	A
43	CPAJ-17	1000	0.67	0.5	42.1	0.3	A
44	CPEN-1	991	4.56	0.5	42.4	0.2	D
45	CPEN-2	953	4.52	0.6	34.9	0.5	D
46	CPEN-3	945	2.09	0.5	41.4	0.2	A
47	CPEN-4	937	4.08	0.4	36.2	1.1	D
48	CPEN-5	928	5.28	0.4	24.7	1.1	D

49	CPEN-7	904	1.53	0.3	27.1	1.2	D
50	CPEN-8	889	5.81	0.7	31.2	1.0	D
51	CCHI-1-1	1088	-1.27	0.4	28.2	1.4	A
52	CCHI-1-2	1078	-2.99	0.4	29.6	0.7	A
53	CCHI-1-3	1065	-0.83	0.4	40.9	0.3	A
54	CCHI-1-4	1055	-1.36	0.7	41.8	0.2	A
55	CCHI-1-6	1035	-1.24	0.6	43.2	0.1	A
56	CCHI-1-8	1015	0.15	0.7	44.7	0.1	A
57	CCHI-1-9	997	0.56	0.6	40.5	0.3	A
58	CCHI-1-10	907	1.24	0.6	43.8	0.1	A
59	CCHI-1-11	918	1.21	0.7	43.2	0.1	A
60	CCHI-1-12	927	0.98	0.4	40.1	0.1	A
61	CCHI-1-13	938	1.17	0.5	40.5	0.2	A
62	CCHI-1-15	958	0.27	0.6	39.0	0.1	A
63	CCHI-1-16	968	0.48	0.6	39.1	0.1	A
64	CCHI-1-18	988	0.99	0.7	39.1	0.2	A
65	CCHI-2-1	962	0.51	0.7	34.2	0.2	A
66	CCHI-2-2	952	1.07	0.6	35.0	0.2	A
67	CCHI-2-3	931	0.09	0.4	32.2	0.2	A
68	QLOA-1	1051	2.30	0.6	32.5	1.0	A
69	QLOA-2	1025	1.49	0.6	32.5	1.0	A
70	QLOA-3	1032	1.00	0.7	40.3	0.4	D
71	QLOA-4	1020	0.63	0.8	37.7	0.3	A
72	QLOA-5	1012	0.94	0.7	43.6	0.3	A
73	QC1-7	1133	-8.9	0.2	37.0	0.7	D
74	QC1-6	1133	-7.4	0.2	33.0	0.6	D
75	QC1-5	1133	-4.7	0.2	33.1	0.6	D
76	QC1-4	1133	-5.8	0.2	30.4	0.6	D
77	QC1-3	1133	-6.6	0.2	32.2	0.9	D
78	QC1-2	1133	-6.7	0.3	38.7	0.4	D
79	QC1-1	1133	-3.0	0.3	39.1	0.4	D
80	CP1-1	967	-4.3	0.2	42.2	0.3	D
81	CP1-2	967	-3.9	0.2	42.2	0.3	D
82	CP1-3	967	-1.9	0.3	41.0	0.4	D
83	CP1-4	967	-1.6	0.4	42.0	0.4	D

<sup>a</sup>Abbreviations according to Table 1

Table S2: Cloud base and cloud top heights offshore averaged over 15 years (2003-2017) was determined using the Multi-angle Imaging SpectroRadiometer (MISR) according to Böhm et al. (2019).

Latitude (°S)	Cloud base height (m)	Cloud top height (m)
23.875	798.82	1235.56
23.625	798.01	1229.65
23.375	783.13	1216.85
23.125	798.61	1230.73
22.875	824.91	1249.18
22.625	818.50	1234.34
22.375	826.60	1230.01
22.125	835.24	1210.93
21.875	813.85	1209.35
21.625	815.13	1194.81
21.375	815.43	1201.28
21.125	830.54	1233.63
20.875	844.07	1243.32
20.625	850.08	1260.62
20.375	845.78	1253.94
20.125	837.19	1239.76
19.875	868.41	1243.58
19.625	860.13	1245.24
19.375	835.23	1251.43
19.125	870.28	1275.25
18.875	866.72	1299.73
18.625	915.78	1327.65
18.375	974.41	1355.56
18.125	863.78	1294.79

Table S3: Pearson correlation coefficients and *p*-values between site-averaged  $\delta^{15}\text{N}$  values of *Tillandsia* plant material and climate variables. Significant correlations are highlighted in bold.

	<b>r</b>	<b>p</b>	<b>n</b>
Latitude	<b>-0.94</b>	<b>0.0004</b>	9
Distance inland	-0.24	0.5624	9
Altitude	0.05	0.8990	9
Cloud base <sup>a</sup>	<b>-0.93</b>	<b>0.0010</b>	9
Cloud top <sup>a</sup>	<b>-0.93</b>	<b>0.0008</b>	9
Cloud cover land <sup>b</sup>	<b>-0.90</b>	<b>0.0023</b>	9
Cloud cover ocean <sup>b</sup>	<b>-0.94</b>	<b>0.0007</b>	9
Aqua 01:30 LT <sup>c</sup>	<b>-0.86</b>	<b>0.0055</b>	9
Aqua 13:30 LT <sup>c</sup>	0.13	0.7504	9
Terra 22:30 LT <sup>c</sup>	-0.46	0.2479	9
Terra 10:30 LT <sup>c</sup>	<b>-0.98</b>	<b>0.0000</b>	9
MAP <sub>WRF</sub> <sup>d</sup>	<b>-0.98</b>	<b>0.0000</b>	9
N (%)	-0.55	0.1573	9
SST (annual mean) <sup>e</sup>	-0.47	0.2378	9
NO <sub>3</sub> <sup>-</sup> (Jan-Mar) <sup>e</sup>	<b>-0.99</b>	<b>0.0004</b>	4
NO <sub>3</sub> <sup>-</sup> (Apr-Jun) <sup>e</sup>	0.90	0.0967	4
NO <sub>3</sub> <sup>-</sup> (Jul-Sep) <sup>e</sup>	0.27	0.7259	4
NO <sub>3</sub> <sup>-</sup> (Oct-Dec) <sup>e</sup>	-0.74	0.2620	4
PO <sub>4</sub> <sup>3-</sup> (Jan-Mar) <sup>e</sup>	<b>-0.99</b>	<b>0.0121</b>	4
SiO <sub>2</sub> (Jan-Mar) <sup>e</sup>	<b>0.96</b>	<b>0.0385</b>	4

<sup>a</sup>MISR product

<sup>b</sup>MODIS product

<sup>c</sup>Satellite with overflight time (local time LT)

<sup>d</sup>modelled mean annual precipitation (Reyers et al., 2019; Reyers, 2019)

<sup>e</sup>surface (0m) ocean data retrieved from world ocean atlas WOA13 (Locarnini et al., 2013)

Fig. S1: Total cloud cover (TCC) over ocean between 71-70.5°W derived from the Terra and Aqua satellites, respectively, recording different overpass times.

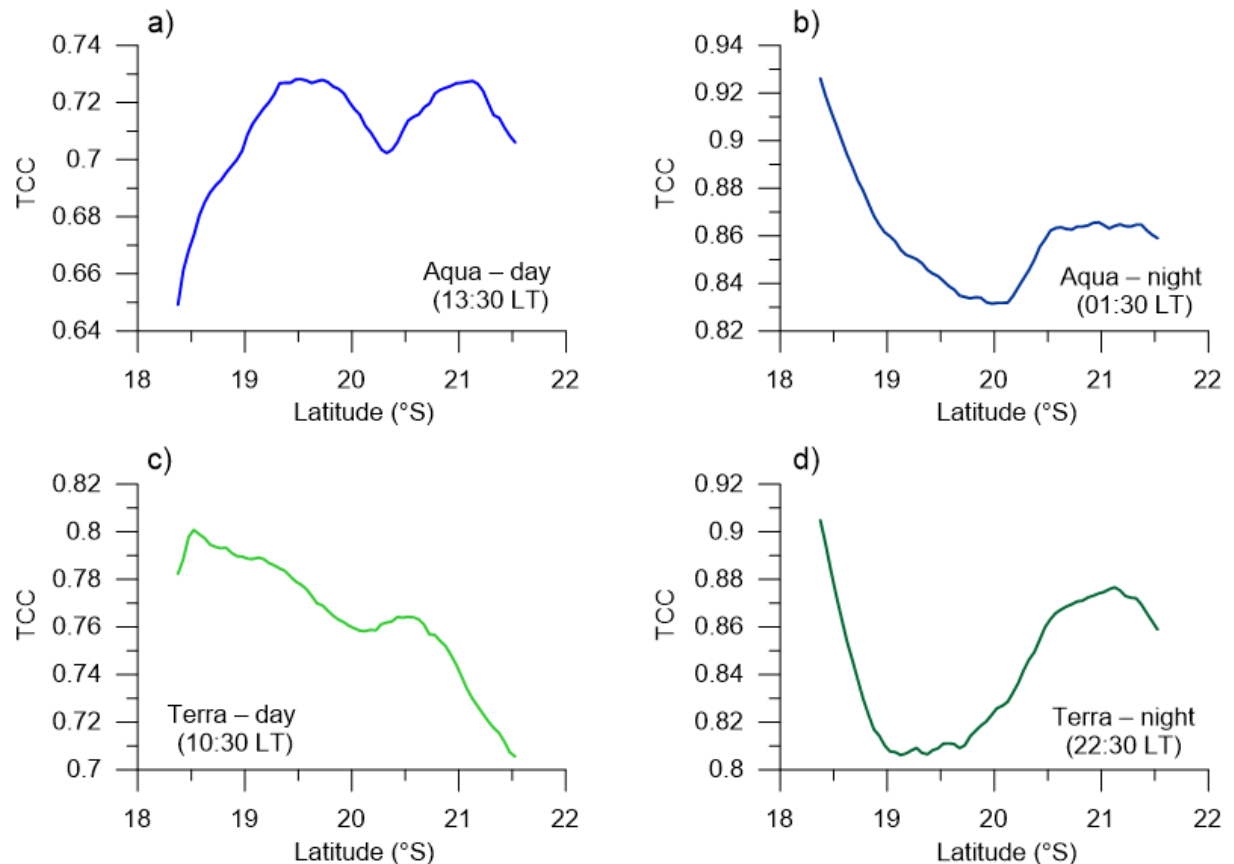


Fig. S2: Total cloud cover (TCC) over land at the specific *Tillandsia* location derived from the Terra and Aqua satellites, respectively, recording different overpass times.

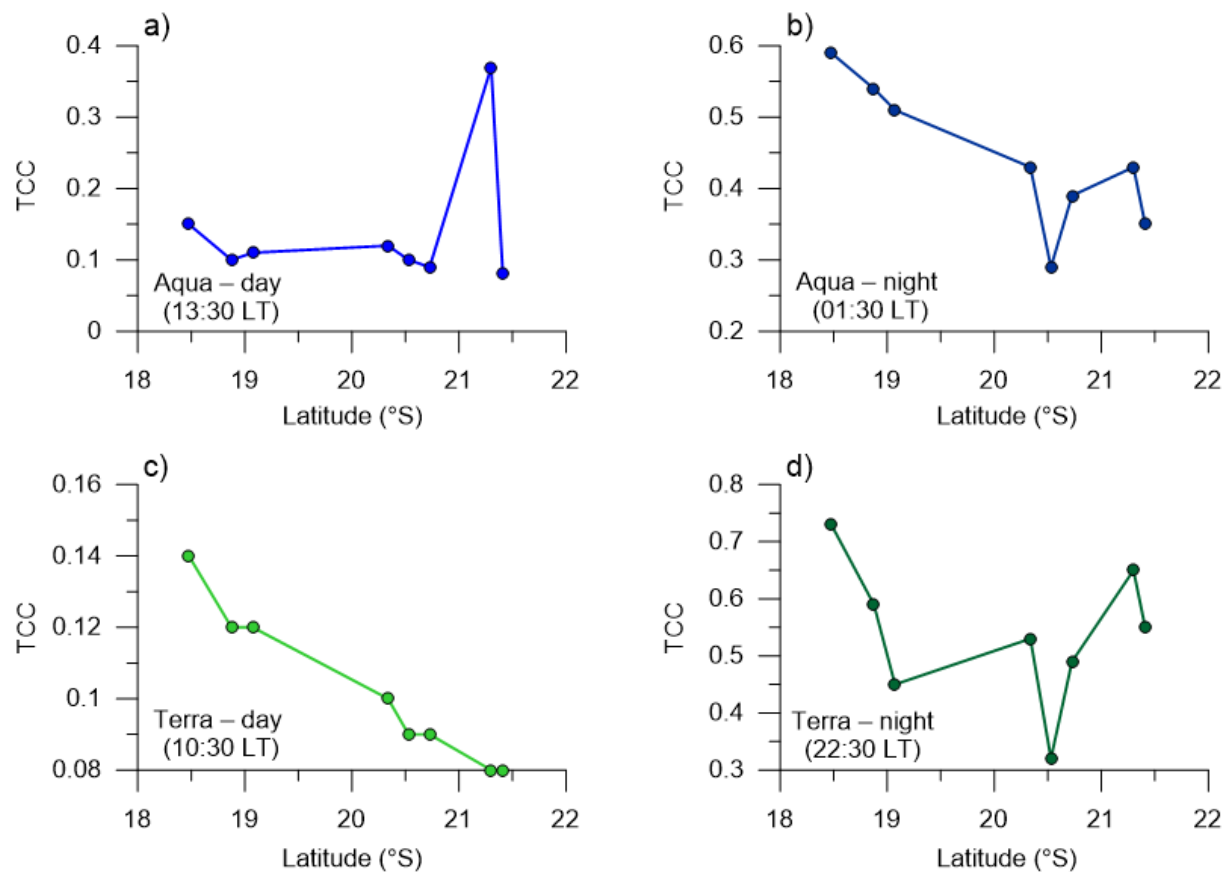


Fig. S3:  $\delta^{13}\text{C}$  values of living *Tillandsia* plant material become more  $^{13}\text{C}$ -enriched with increasing distance to the coast and may indicate higher water stress further inland.

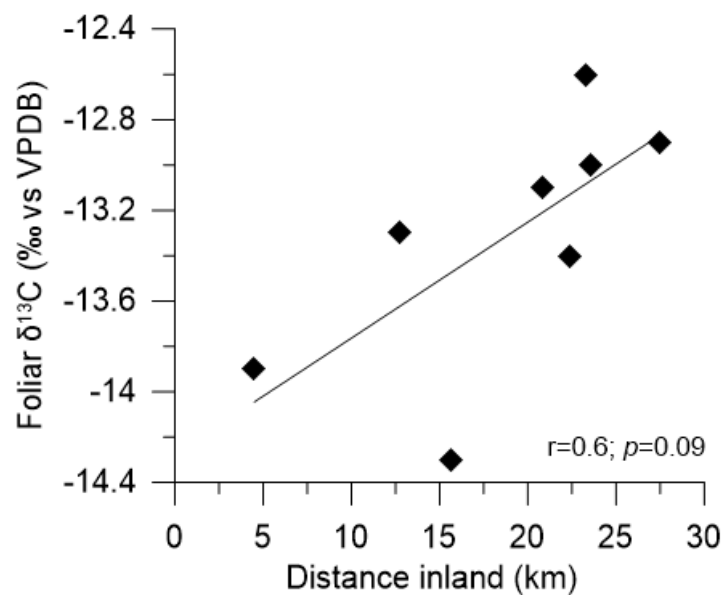


Fig. S4: Chronology of dune evolution based on radiocarbon ages of relict *T. landbeckii* layers at Cerro Pajonales and Quebrada Camarones, respectively.

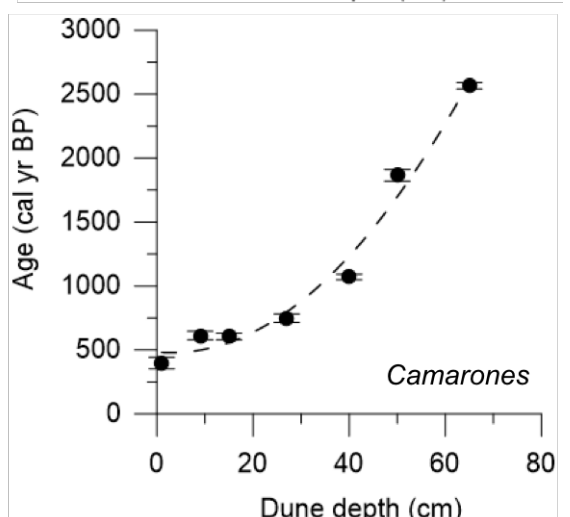
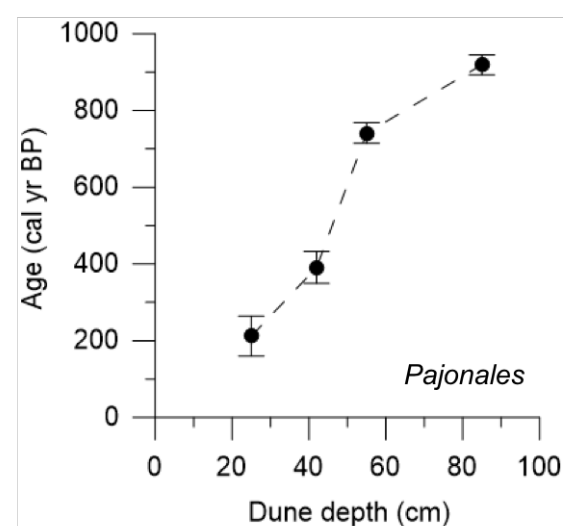
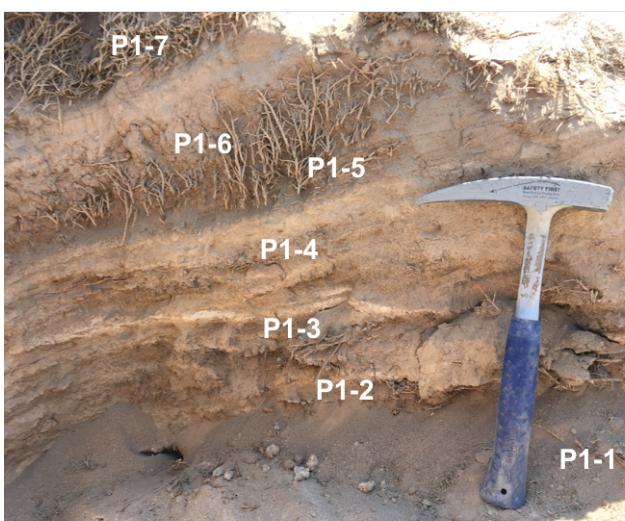
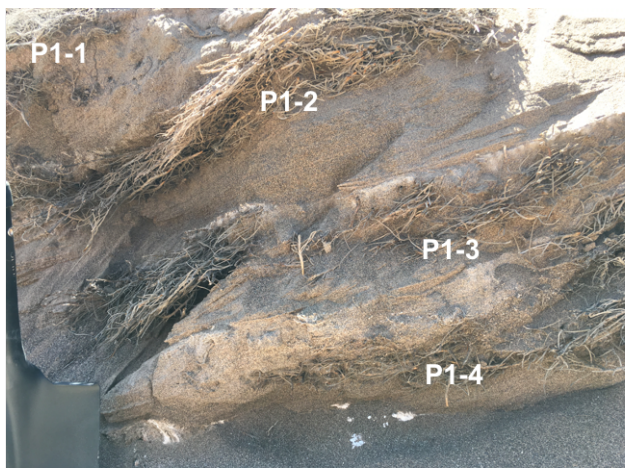


Fig. S5: Range in  $\delta^{15}\text{N}$  values for different plant species in the Atacama Desert and for some common reservoirs (modified after Sharp, 2014). Grey bars indicate  $\delta^{15}\text{N}$  values of dead *Tillandsia* specimen.

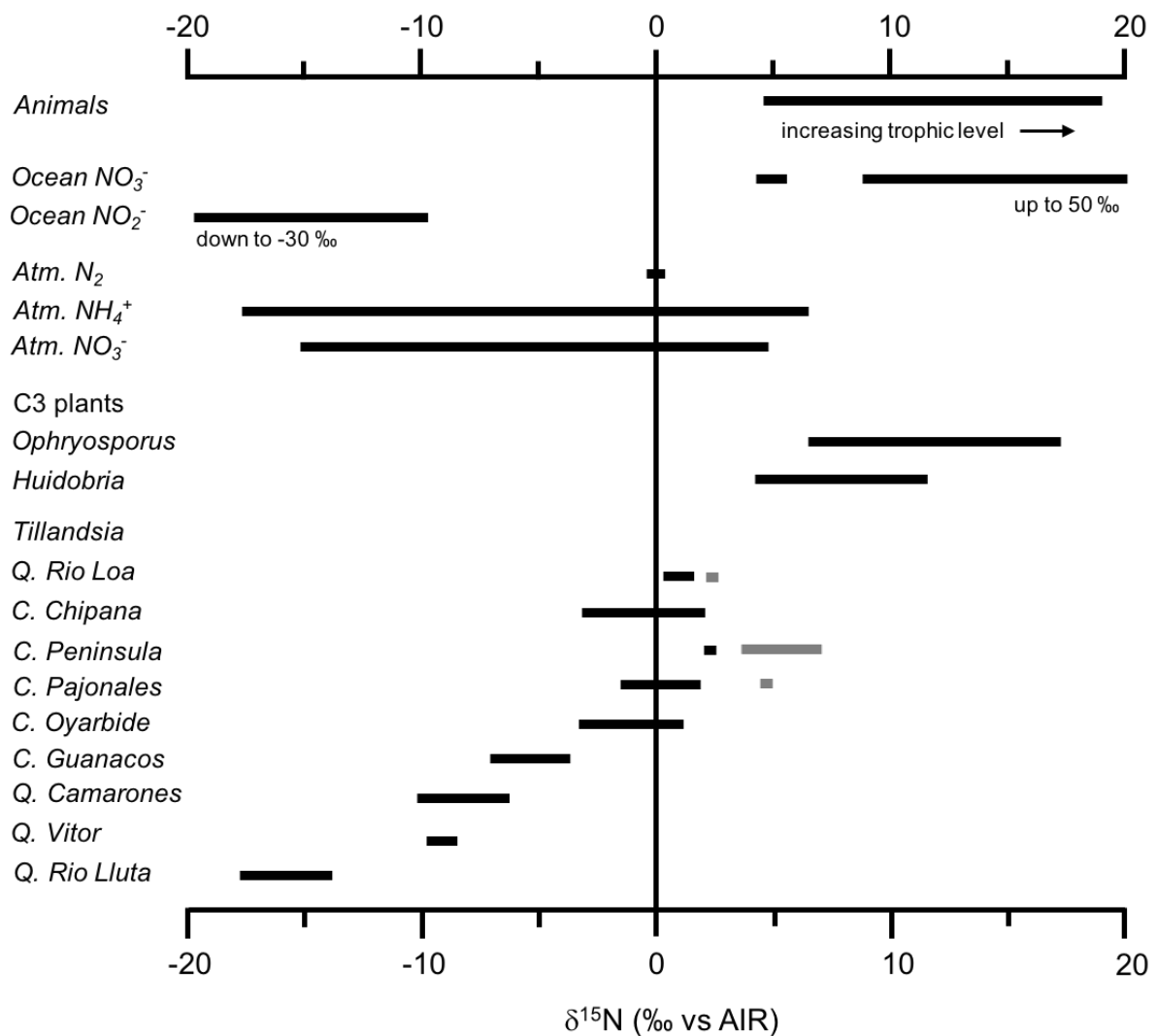


Fig. S6: Map showing the distribution of  $\delta^{15}\text{N}$  values of all living plants investigated in this study.

